The Initial Corrosion Behaviour of Galvanized Reinforcing Bar in Concrete

Zuo Quan Tan[1], Carolyn M. Hansson[2]

Abstract

Hot dip galvanized reinforcing bar is used to prolong the service life of reinforced concrete structures exposed to chlorides and/or carbonation. While the protection afforded by the zinc in the long term has been adequately demonstrated, there have been concerns about the initially high corrosion rate of the zinc when it is exposed to the highly alkaline fresh concrete. The issues of concern are (i) that it could lead to excessive loss of coating, rendering the galvanic protection ineffective in the long term; (ii) any increased porosity of the concrete adjacent to the rebar because of the hydrogen evolved during corrosion which could lead to loss of bond strength between the bar and the concrete and (iii) the need for chromating to minimize the first two issues. The results have shown that the coating loss is insignificant in ordinary Portland cement concrete, but is considerably higher in concretes containing either silica fume or ground granulated blast furnace slag. Nevertheless, in all cases, chromating was not found to be necessary and no increase in porosity adjacent to the steel could be detected using mercury intrusion porosimetry.

Keywords: galvanized rebar, corrosion, concrete, porosity, hydrogen

Introduction

Premature deterioration of concrete structures due to corrosion of carbon steel reinforcing bars (rebars) is a major problem in areas where de-icing salts are used extensively in winter. Galvanized steel reinforcements, which were introduced in the 1930s [1], are aimed at prolonging the service life of such structures [2] by increasing the chloride concentration necessary for corrosion initiation [3] and, therefore, the time to initiate corrosion and reducing the subsequent rate of corrosion. The zinc coating on hot-dip galvanized (HDG) steel reinforcing bar (rebar) has two purposes. First, it covers the steel surface and prevents aggressive species such as chloride ions, moisture and oxygen that are responsible for corrosion, from reaching the underlying steel [4]. Second, in cases where the steel is exposed, the galvanic reaction of the zinc reduces the corrosion rate of the steel.

Zinc is highly corrosive in alkaline solutions and reacts strongly when exposed to fresh concrete. However, the product of corrosion in concrete pore solution is calcium hydroxyzincate (CHZ) which, at pH less than ~13.3, has been shown to reduce the corrosion rate to insignificant levels. The pH in concrete is often higher than this level and, therefore, concern has been expressed that the initial corrosion could lead to (a) excessive loss of coating, rendering the galvanic protection ineffective in the long term and (b) increased

[1] Engineering Intern Training, The Greer Galloway Group Inc., Canada
[2] Professor, Mechanical and Mechatronics Engineering, University of Waterloo, Canada

porosity of the concrete adjacent to the rebar because of the hydrogen evolved during corrosion. A third concern is the currently perceived need for chromating to minimize the first two issues, because of the toxicity associated with chromates.

This paper addresses these issues and investigates the influences of galvanized coating surface condition and concrete mix design on the initial corrosion behaviour.

Experimental Procedure

The initial corrosion behaviour in concrete of hot dip galvanized rebar was evaluated for bars with the following four surface conditions:

1. "Non-chromated bar": with a pure zinc surface layer and iron-zinc alloy subsurface layers;
2. "annealed bar" with a coating consisting only of Fe-Zn alloy layers;
3. "weathered bar" initially with a pure zinc surface layer but exposed outdoors for several months to produce a layer containing zinc oxide and zinc carbonate;
4. "chromated bar" with a pure zinc surface layer with a chromate surface film applied through immersion in a dilute chromic acid solution immediately after galvanizing.

Five bars in each condition were tested in ordinary Portland cement concrete (OPCC) and five specimens of the non-chromated and chromated bars were tested in the concretes containing silica fume or ground granulated blast furnace slag. The concrete mixture proportions are given in Table 1.

A schematic diagram of the concrete cylinders with the embedded electrodes is shown in Figure 1. The cylinders were 100 mm ø by 200 mm. The HDG bar and graphite counter electrode were partially painted with epoxy to give the same exposed length allowing the exposed zinc surface to be uniformly polarized. The graphite "reference electrode" was partially painted to give a smaller exposed area, as shown, to minimize fluctuations in its potential. The graphite electrodes were positioned 10 mm away from the HDG bar; this distance is greater than the maximum aggregate size of 7 mm to ensure free flow of concrete during casting and compaction to prevent damage to the electrodes by aggregates.

Immediately after embedding the bars in concrete, the corrosion rates were monitored at hourly intervals for the first two days. Corrosion monitoring was achieved using a data acquisition system [5]. Potentiostatic linear polarization resistance, LPR with a scan range of ±20mV with respect to the open circuit potential was used and the corrosion current density i_{corr} was calculated using the Stern-Geary formula [6]. The values of B have been determined experimentally for active and passive corrosion of the HDG bar to be 39mV and 20mV respectively [7].

In addition, cylindrical cement paste specimens, of the same proportions as the concrete, but without the aggregates, were cast with a central HDG bar and cured for nine days. They were then sectioned to provide specimens as shown in Figure 2 for mercury intrusion porosimetry (MIP) and environmental scanning electron microscopy (ESEM) with energy dispersive x-ray spectroscopy (EDS). These were used to determine the porosity of the paste adjacent to the bar and the diffusion of zinc corrosion products into the paste, respectively.

For the MIP, each specimen was weighed and then submerged into isopropyl alcohol for 24 hours, allowing water in the cement pores to be replaced. The specimens were then withdrawn from the alcohol and put under a vacuum to allow the alcohol to evaporate. As the weight of the specimens was stabilized when evaporation was complete, the process was

repeated until the weight of the specimens remained constant. Prior to performing MIP, the specimens were kept in a vacuum desiccator to prevent further hydration of the specimens. Three specimens from each cylinder were prepared and tested using MIP.

For ESEM/EDS, the specimens were prepared as above and then mounted in epoxy with the top surface of the section illustrated in Figure 2 exposed, which was polished flat for observation and analysis.

Results and Discussion

The influence of surface composition on initial corrosion

The corrosion rates of the different bars in OPC concrete as a function of time after casting are shown in Figure 3. These data must be interpreted in light of the hydration of the cement, which is occurring simultaneously. Upon concrete mixing, the mixing water becomes saturated with Ca^{2+} and OH^- ions and also contains SO_4^{2-}, K^+, and Na^+, causing a sudden increase in electrical conductivity and pH, and thereby, an initial increase in corrosion current. The subsequent decrease in corrosion rates can be attributed to a combination of (i) CHZ formation, (ii) lower ionic activity during the dormant period of cement hydration and (iii) a constriction of the initial mixing water into the developing pore structure of the cement paste.

Immediately after casting, the non-chromated bars exhibited the greatest scatter in corrosion rates, varying between 27 and 75 $\mu A/cm^2$. This is probably a result of non-uniform composition at the surface caused by the hot-dip process in which all the bars were immersed together in the zinc bath and then lifted out and quenched in cold water. It is possible that some experienced a faster quenching rate than others, resulting in different grain sizes and compositions at the surface. Overall, however, these bars had less active corrosion than the other bars.

The annealed bars exhibited the highest initial corrosion rate due to the presence of iron in the intermetallic phase at the surface. This rate decreased and reached a plateau after about 5 hours, decreasing only gradually until the protective CHZ formed on the surface. The weathered bars had the lowest initial corrosion rate which is attributed to the oxide and carbonate products providing a barrier to the pore solution. However, the barrier is rapidly broken down and, after about two hours, these bars had the highest corrosion rates, between 85 and 95 $\mu A/cm^2$ and the longest period of active corrosion before the protective CHZ layer developed. The maximum corrosion rate of the chromated bars was also delayed but active corrosion halted before that of the annealed or weathered bars. The amount of zinc loss, calculated from the area under the curves is given in Table 2.

The effect of concrete type on initial corrosion rate

The corrosion current densities of chromated and non-chromated HDG bars in silica fume and in slag concrete are plotted as a function of time after casting for the initial two days in Figures 4 and 5, respectively. While the initial behaviour of the chromated bars is similar to those in OPCC, the non-chromated bars exhibited higher corrosion rates. This was particularly evident for the bars in the slag cement. In this case, the very high corrosion rates may be attributed to the fact that slag would not have begun to react in this period and,

therefore, the effective water-to-binder ratio would have been much higher than in the OPCC, allowing greater ionic mobility and faster corrosion. Also, in the silica fume concrete, the non-chromated bars exhibited a second peak in corrosion current, which was not observed for these bars in OPCC.

From the corrosion data presented here it is clear that for the initial active corrosion during the early hydration of silica fume and slag concrete, chromate treatment improved the resistance to corrosion for HDG bars. Nevertheless, in both silica fume and slag concrete, neither type of bar achieved the low levels of corrosion observed in the OPCC within the first two days. Therefore, the corrosion was monitored for a longer period to determine if corrosion protection developed over time.

For bars in silica fume concrete, the corrosion was monitored at selected times, up to a period of one month. As shown in Figure 6, the corrosion rates gradually decreased over time. However, at the end of one month, the corrosion current densities were still of the order of 1 – 3 $\mu A/cm^2$. Nevertheless, based on the decreasing trend, it is reasonable to assume that over time, passivation would occur.

For the slag concrete specimens, Figure 7, corrosion was monitored for approximately eighteen days. After four days, the corrosion of the non-chromated bars reached levels of ~1 $\mu A/cm^2$, whereas the chromated bars continued to corrode at a higher level (~6 $\mu A/cm^2$).

Table 3 summarizes the corrosion and depth loss for all bars in the three types of concrete used. Due to higher corrosion rates in silica fume concrete, the average coating depth losses for non-chromated and chromated bars were 6.5 and 2.4 times higher than those in OPC concrete for the initial two days. Over the initial month, both the chromated and non-chromated bars lost significant amounts of their coating in silica fume concrete.

Porosity and zinc in the cement adjacent to the rebar

The porosity of the cement adjacent to the non-chromated and chromated steels in the three cements is illustrated by plots of the cumulative intrusion volume of mercury versus pore radius, in Figures 8 - 10. Also included in Figure 8 are the data for uncoated (black) steel in OPC. It is evident that there is a discontinuity in the cement pore size distribution adjacent to the black steel in the range of 0.02 to 0.1 μm which was not observed in the cements adjacent to the HDG bars. It is generally believed that a layer of calcium hydroxide is deposited at steel bar/cement interface [8], and this pore size range may represent the pores in the $Ca(OH)_2$ layer. For specimens adjacent to HDG bars, this layer may not exist, or be present at a lower quantity, as it would have been consumed during the formation of CHZ. For both the silica fume and slag cements, a similar but less pronounced discontinuity was also observed, probably because less CHZ was formed in these cements than in OPC and, therefore, less of the calcium hydroxide layer was consumed. Moreover, the porosity in this range is greater for the paste adjacent to the chromated steel than in that next to the non-chromated steel. Since the chromating prevents the formation of CHZ in the early stages this again supports the theory that the additional porosity in the 0.02 to 0.2μm range is due to the interfacial layer of $Ca(OH)_2$.

The total intruded volume for the different cements is given in Table 4. Regardless of the type of cement, there was insignificant difference in cumulative intrusion volume between the cement pastes adjacent to chromated and non-chromated bars. However, amongst the different cement types, both the silica fume and slag cement had the lower intrusion volumes

than the OPC cement, which was expected as silica fume and slag are known to form additional C-S-H which reduces the pore space.

The higher intrusion volume of the cement adjacent to uncoated bars, compared to those adjacent to HDG bars suggests that the zinc corrosion products may be diffusing into the cement pores. This hypothesis is confirmed by ESEM/EDS observations. Figures 11-16 are ESEM micrographs of cross sections of the cement paste adjacent the steel on which are superimposed the zinc contents from EDS spot analysis. The cement/steel interface is on the left of each figure. The zinc content is reported in weight percent of all the elements detected within the location of analysis. A zinc content of 1% or less is considered negligible since it falls within the error range of detection.

For OPC cements, the depths of diffusion are no more than 500□m and the type of bar does not seem to have an effect on this depth. The lower porosity of the silica fume cement resulted in a considerably lower diffusion depth than that in OPC cement. The diffusion depth of the slag cement is comparable to the silica fume cements. The zinc contents near the chromated bar/slag cement interface, however, are significantly higher than in the other specimens. Since only one cement sample was examined, conclusive comments cannot be made regarding this observation.

Regardless of the differences in diffusion depths and zinc contents observed for the different cements, the data confirmed that corrosion products did, in fact, diffuse into the cement, and therefore, also confirmed the hypothesis that the lower porosity for cement adjacent to HDG bars compared to cement adjacent to an uncoated steel bar is, in fact, due to the diffusion of corrosion products.

Conclusions

- The loss of zinc coating due to the initial active corrosion of the HDG reinforcing bars with all four surface conditions in OPCC was found to be negligible (≤ 2μm) and insufficient to jeopardize the long term protection provided by the coating.
- The loss of zinc coating thickness in concrete containing slag and silica fume is more problematic. The reasons for the increased corrosion and lower longer-term protection provided by these materials are currently being investigated. It is anticipated that, when these are determined, methods of amelioration can be proposed.
- Hydrogen evolution does not result in increased porosity in the cement paste adjacent to the steel, irrespective of the cement composition. This is attributed, at least in part, due to diffusion of zinc corrosion products into the surrounding cement paste.
- Chromating does not improve the corrosion resistance of HDG bar in OPCC.
- Chromating reduces the initial corrosion of HDG bar in both slag cement concrete and silica fume concrete. However, the chromated bars in the slag cement concrete exhibit higher corrosion rates than the non-chromated bars after the first two days.
- Consequently, chromating has been shown to be unnecessary and, because of the health problems associated with chromates, is not recommended.

Acknowledgments

The authors gratefully acknowledge the financial support for this project provided by the City of Calgary, Alberta, Canada and the International Lead Zinc Research Organization. The assistance of Dr. Amir Poursaee in the electrochemical measurements is greatly appreciated.

References

1. YEOMANS, S.R., Performance of black, galvanized and epoxy-coated reinforcing steels in chloride-contaminated concrete. Corrosion, 1994. 50(1): p. 72-81.

2. YEOMANS, S.R. Comparative studies of galvanized and epoxy coated steel reinforcement in concrete. in Durability of Concrete-Second International Conference. 1991. Montreal, Canada.

3. ANDRADE, C., ALONZO, C., Electrochemical Aspects of Galvanized Steel, in Galvanized Steel Reinforcement in Concrete, S.R. YEOMANS, Editor. 2004, Elsevier. p. 111-143.

4. BELAÏD, F., ARLIGUIE, G., FRANCOIS, R., Porous structure of the ITZ around Galvanized and ordinary steel reinforcement Cement and Concrete Research, 2001. 31: p. 1561-1566.

5. POURSAEE, A., Automatic Corrosion Monitoring System for Steel Reinforced Concrete submitted to Materials Performance.

6. STERN, M., GEARY, A. L., Electrochemical polarization: I. A theoretical analysis of the shape of polarization curves. Journal of Electrochemical Society, 1957. 104(1): p. 55-63.

7. TAN, Z.Q., HANSSON, C.M., Effect of surface condition on the initial corrosion of galvanized reinforcing steel embedded in concrete. Submitted to Corrosion Science.

8. PAGE, C.L., TREADAWAY, K. W. J., Aspects of Electrochemistry of Steel in Concrete. Nature, 1982(297): p. 109-115.

Table 1. Concrete mixture proportions.

Component	OPC Concrete	Silica Fume Concrete	Slag Concrete
Cement	390 kg type 10	390 kg type 10 SF	292 kg type 10 + 98 kg slag
Coarse aggregate (≤ 7 mm)	1100 kg	1100 kg	1100 kg
Fine aggregate	735 kg	735 kg	735 kg
Water	176 l	176 l	176 l
Air entraining agent	234 ml	234 ml	234 ml

Table 2. Corrosion current and depth loss summary within the first two days in OPCC.

Bar Type	Max. active i_{corr} ($\mu A/cm^2$)	Min. passive i_{corr} ($\mu A/cm^2$)	Average depth loss @ 50 hours (μm)
Weathered	83-95	0.6-0.8	2.03
Annealed	41-80	0.2-0.6	1.18
Chromated	37-65	1.1-2.3	0.92
Non-chromated	30-92	0.5-0.7	0.45

Table 3. Corrosion current and depth loss summary in all concrete types.

Concrete	Bar type	Max. i ($\mu A/cm^2$)	Min. i ($\mu A/cm^2$)		Average Depth Loss (μm)	
			@ 2 Days	Extended	@ 2 Days	Extended
OPCC	Non-Chromated Bars	20-50	0.7-1.0	-	0.4	-
	Chromated Bars	25-38	1.5-3.0	-	0.7	-
Silica Fume	Non-Chromated Bars	60-90	15.4-26.7	0.9-3.2 @ 32 days	2.6	9.8 @ 32 days
	Chromated Bars	30-50	8.8-15.0	1.7-3.6 @ 32 days	1.7	6.9 @ 32 days
Slag	Non-Chromated Bars	220-330	6.3-8.8	1.1-1.3 @ 20 days	4.2	5.9 @ 20 days
	Chromated Bars	20-35	4.1-13.4	6.2-6.7 @ 20 days	1.0	9.5 @ 20 days

Table 4. Summary of mercury intrusion volume.

Cement type	Bar type	Average intrusion volume, mm^3/g	Standard deviation
OPC	Black steel bar	226	12.2
	Non-chromated bar	194	17.5
	Chromated bar	206	18.5
Silica fume	Non-chromated bar	134	2.1
	Chromated bar	137	5.2
Slag	Non-chromated bar	155	9.2
	Chromated bar	154	8.9

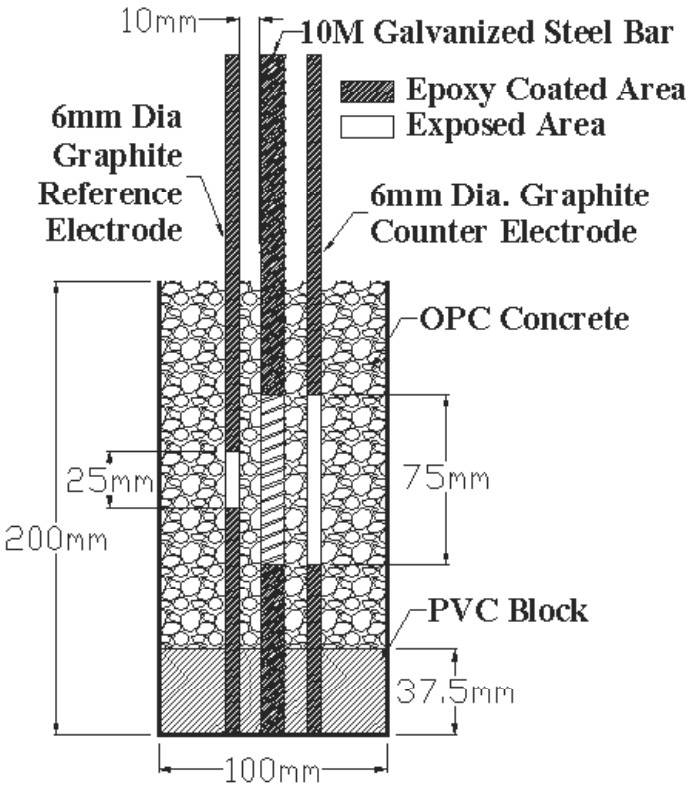

Figure 1. Schematic diagram of corrosion monitoring setup.

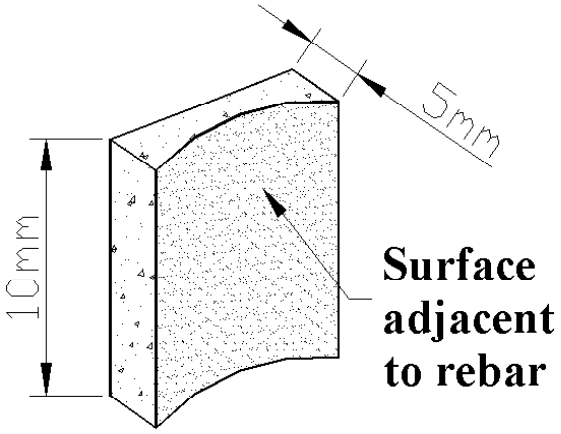

Figure 2. Cement specimen for mercury intrusion porosimetry.

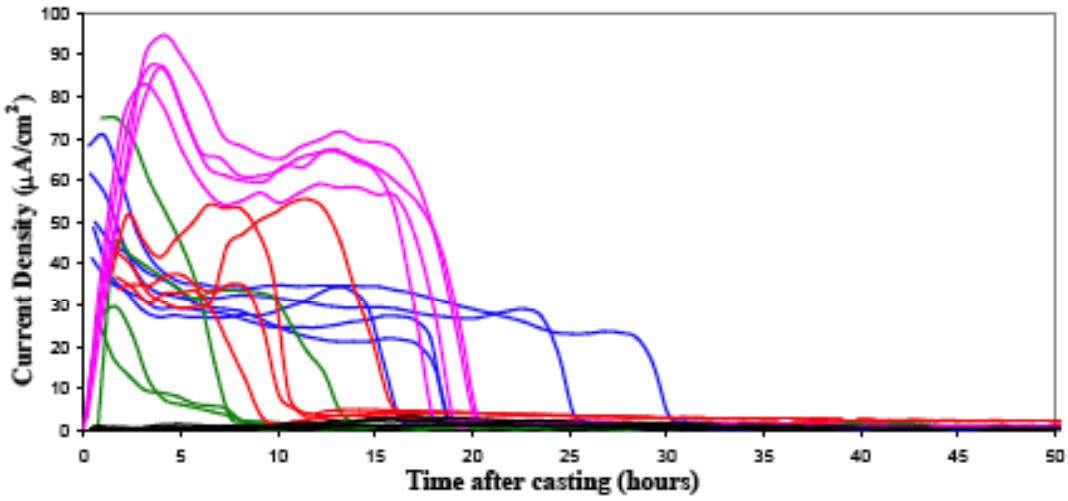

Figure 3. Corrosion of all bars in OPCC: Uncoated, Weathered, Chromated, Non-chromated, Annealed.

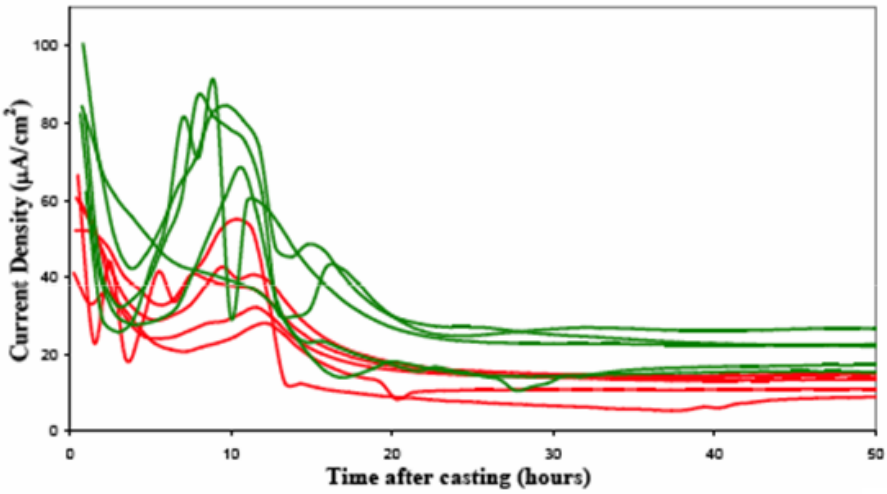

Figure 4. Corrosion of chromated and non-chromated bars in silica fume concrete in the initial two days: Chromated, Non-chromated.

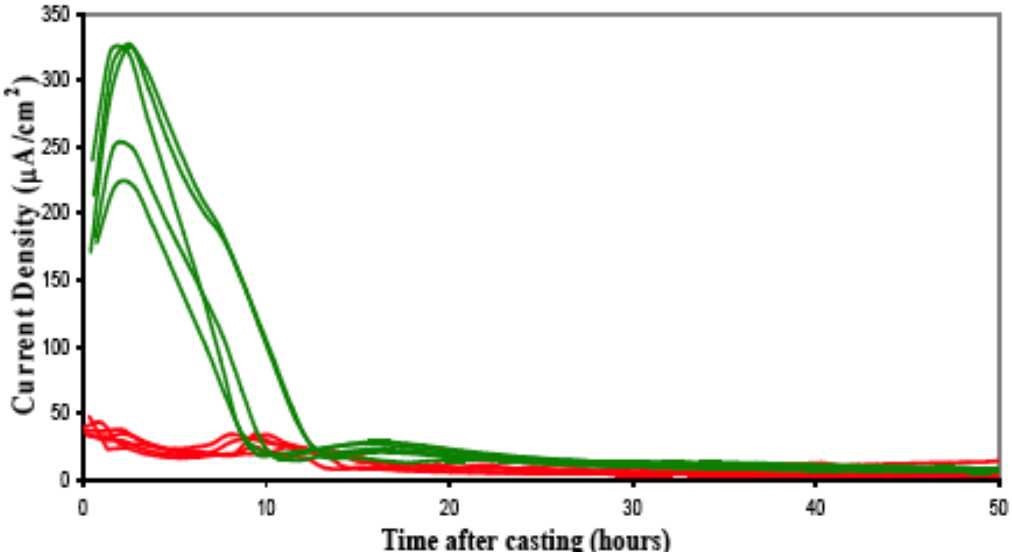

Figure 5. Corrosion of chromated and non-chromated bars in slag concrete in the initial two days: Chromated, Non-chromated.

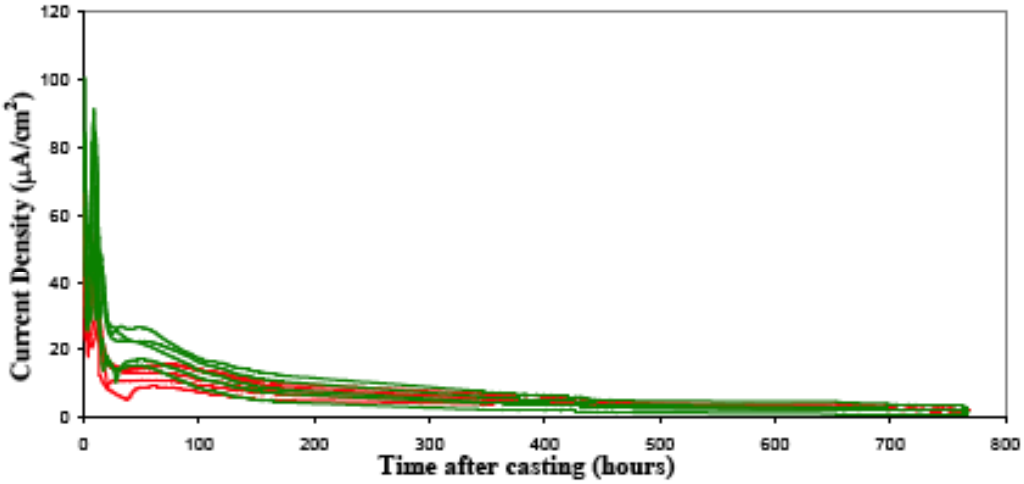

Figure 6. Extended corrosion monitoring of chromated and non-chromated bars in silica fume concrete: Chromated, Non-chromated.

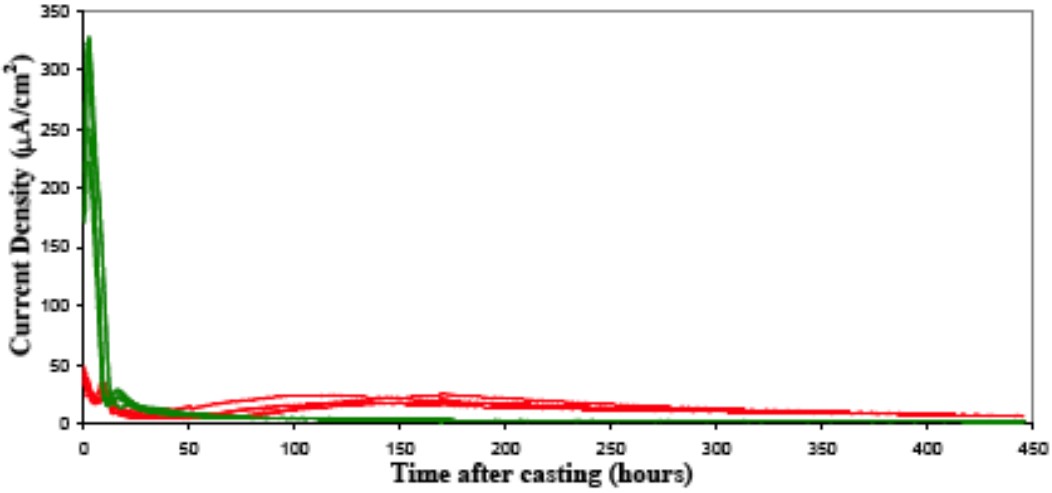

Figure 7. Extended corrosion monitoring of chromated and non-chromated bars in slag concrete: Chromated, Non-chromated.

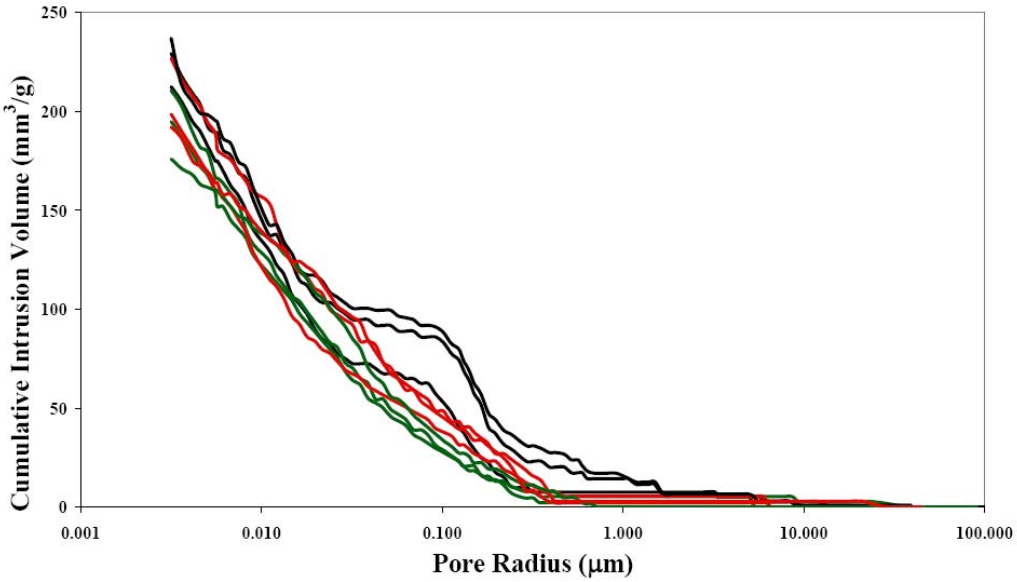

Figure 8. Mercury intrusion plots for OPC pastes: Chromated, Non chromated, Uncoated.

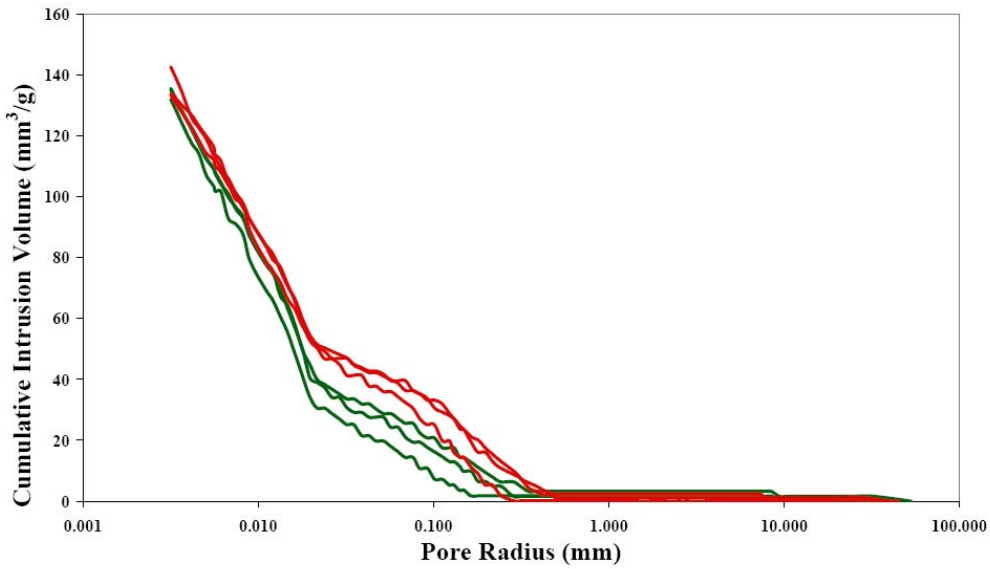

Figure 9. Mercury intrusion plots for silica fume pastes: Chromated, Non-chromated.

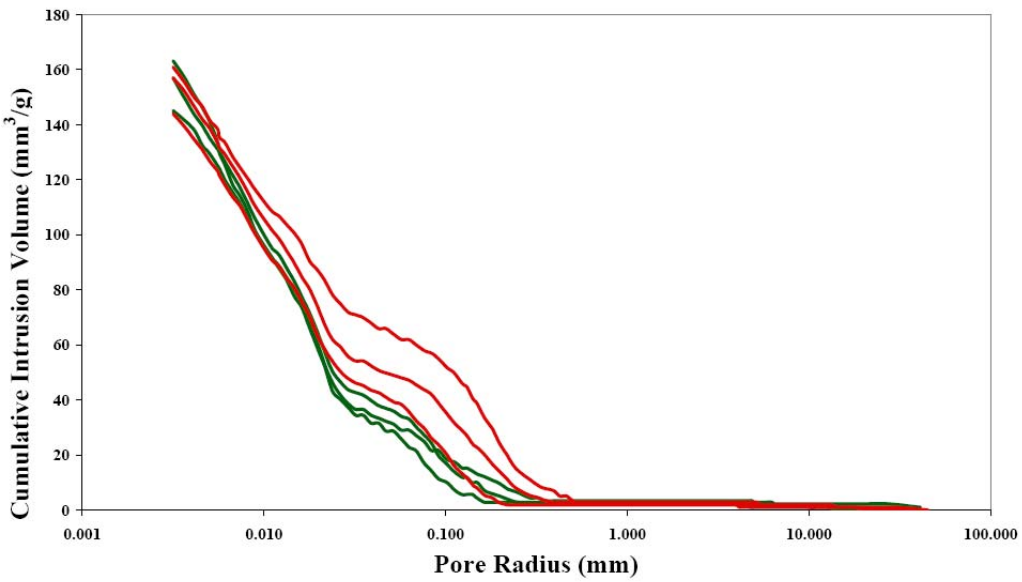

Figure 10. Mercury intrusion plots for slag pastes: Chromated, Non chromated.

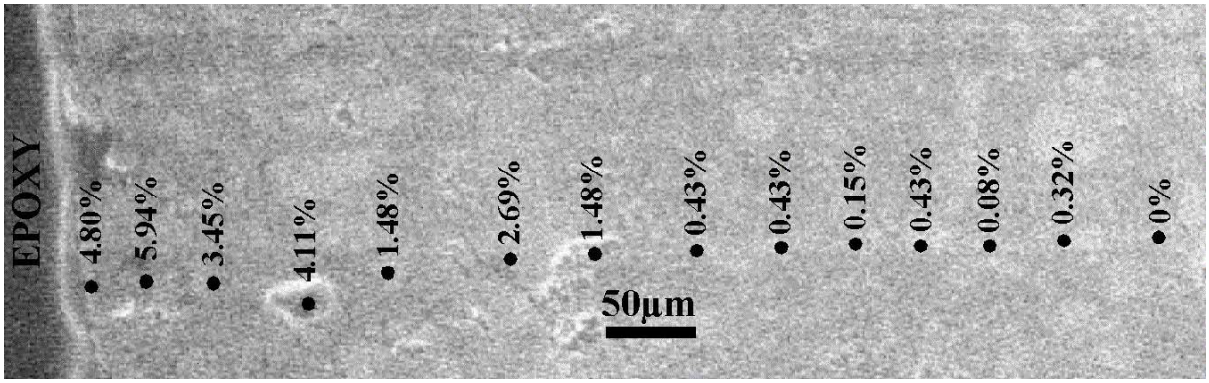

Figure 11. Zinc profile of OPC paste adjacent to a non-chromated bar.

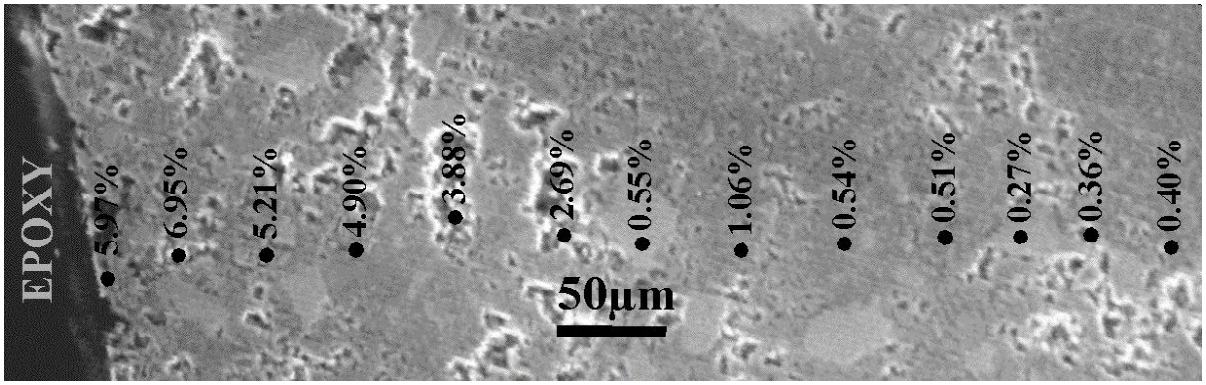

Figure 12. Zinc profile of OPC paste adjacent to a chromated bar.

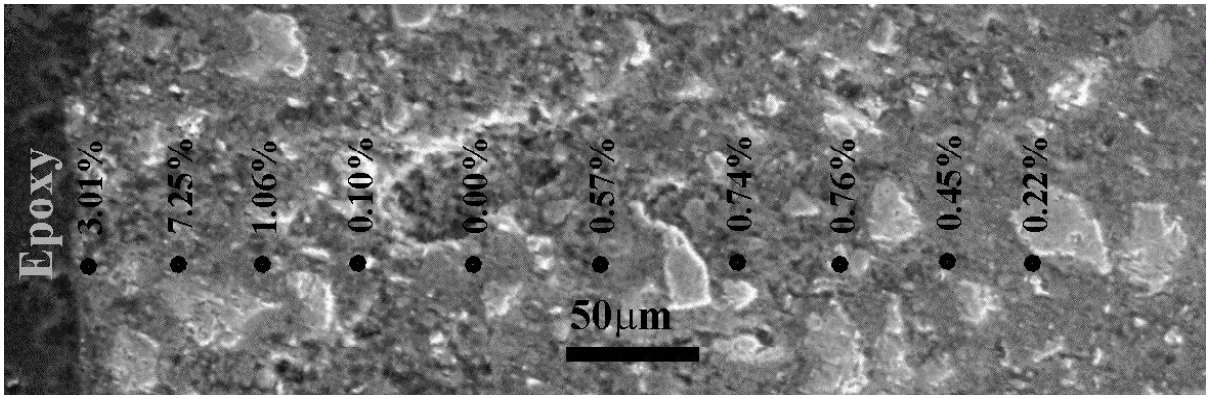

Figure 13. Zinc profile of silica fume cement paste adjacent to a non-chromated bar.

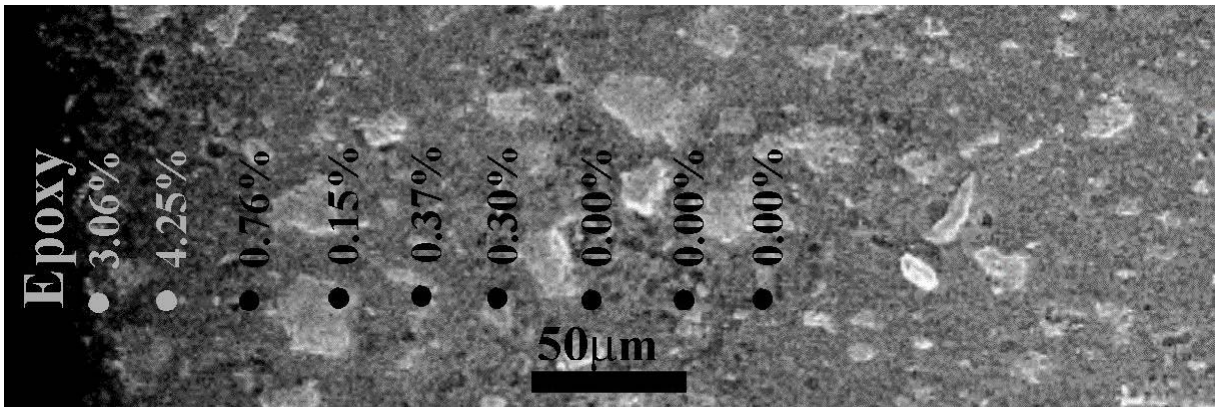

Figure 14. Zinc profile of silica fume cement paste adjacent to a chromated bar.

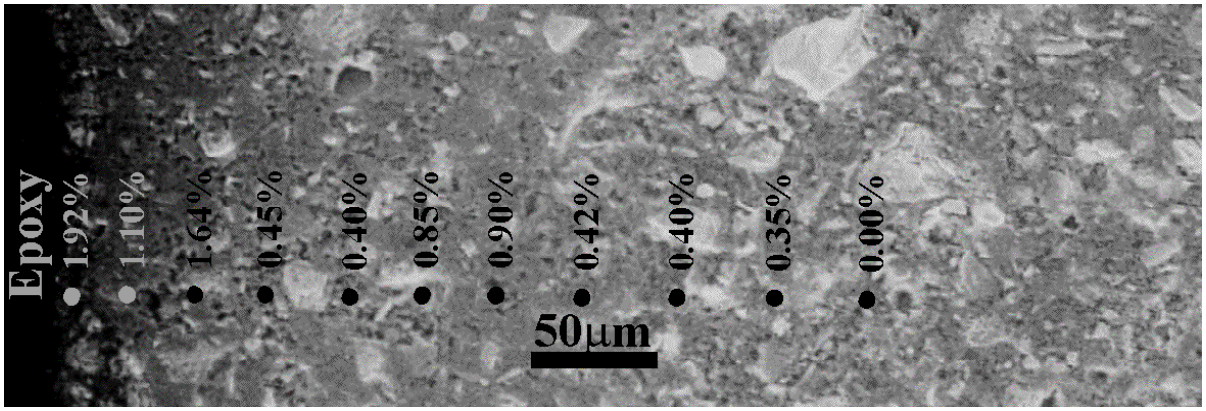

Figure 15. Zinc profile of slag cement paste adjacent to a non-chromated bar.

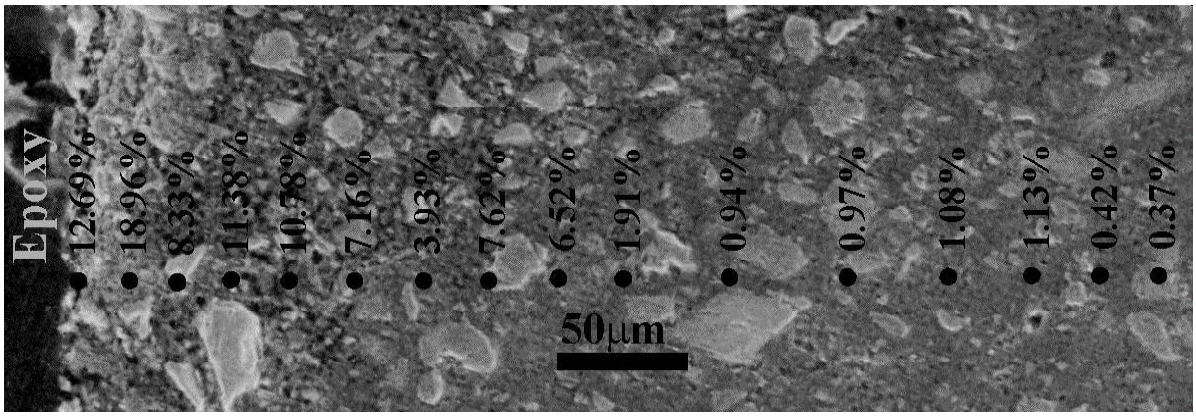

Figure 16. Zinc profile of slag cement paste adjacent to a chromated bar.